DFG-Schwerpunktprogramm 1324

„Extraktion quantifizierbarer Information aus komplexen Systemen”

Efficient and accurate computation of spherical mean values at scattered center points

T. Görner, R. Hielscher, S. Kunis

Preprint 113

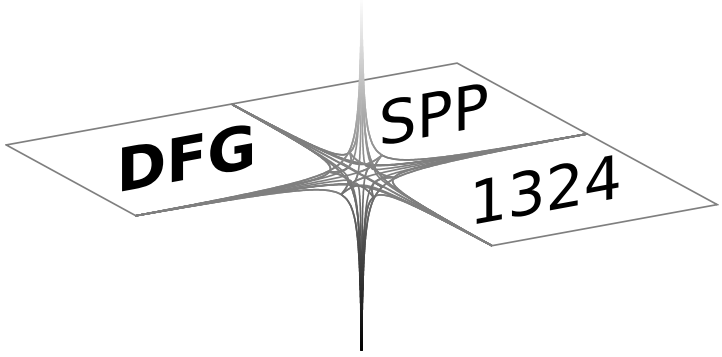

Edited by

AG Numerik/Optimierung
Fachbereich 12 - Mathematik und Informatik
Philipps-Universität Marburg
Hans-Meerwein-Str.
35032 Marburg

DFG-Schwerpunktprogramm 1324

„Extraktion quantifizierbarer Information aus komplexen Systemen”

Efficient and accurate computation of spherical mean values at scattered center points

T. Görner, R. Hielscher, S. Kunis

Preprint 113

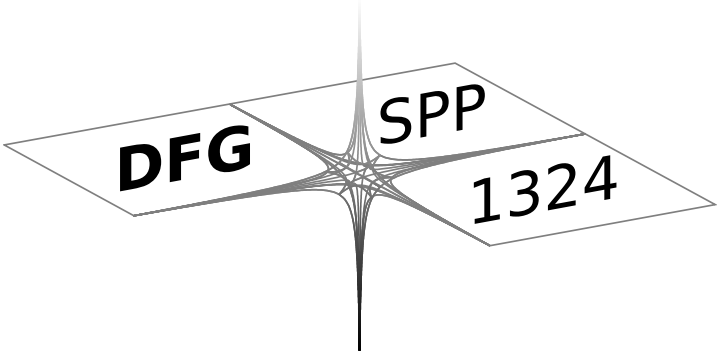

The consecutive numbering of the publications is determined by their chronological order.

The aim of this preprint series is to make new research rapidly available for scientific discussion. Therefore, the responsibility for the contents is solely due to the authors. The publications will be distributed by the authors.

Efficient and accurate computation of spherical mean values at scattered center points

Torsten Görner * Ralf Hielscher† Stefan Kunis‡

Abstract

Spherical means are a widespread model in modern imaging modalities like photoacoustic tomography. Besides direct inversion methods for specific geometries, iterative methods are often used as reconstruction scheme such that each iteration asks for the efficient and accurate computation of spherical means. We consider a spectral discretisations via trigonometric polynomials such that computation can be done via nonequispaced fast Fourier transforms. Moreover, a recently developed sparse fast Fourier transform is used in the three dimensional case and gives optimal arithmetic complexity. All theoretical results are illustrated by numerical experiments.

Key words and phrases : spherical mean operator, trigonometric approximation, fast Fourier transform, tomography.

2010 AMS Mathematics Subject Classification : 65T40, 65T50, 44A12, 92C55.

1 Introduction

In analogy to the classical Radon transform, we consider the spherical mean value operator $\mathcal{M}$ that assigns to each function $f\colon \mathbb{R}^d \to \mathbb{R}$ its mean values

$$\mathcal{M}f(\mathbf{y}, r) := \frac{1}{\omega_{d-1}} \int_{\mathbb{S}^{d-1}} f(\mathbf{y} + r\boldsymbol{\xi}) \, \mathrm{d}\sigma(\boldsymbol{\xi})$$

along the spheres with center point $\mathbf{y}$ and radius r, where σ denotes the surface measure on the sphere and $\omega_{d-1} = \sigma(\mathbb{S}^{d-1})$. The spherical mean value operator plays a equally prominent role for recent imaging techniques as the classical Radon transform does already for about 50 years. Most notably, the mathematical models behind upcoming hybrid imaging techniques like thermo– and photo–acoustic tomography [22, 15, 4] are based upon the spherical mean value operator. In most cases, the inverse problem is of interest, i.e. given the spherical means $\mathcal{M}f(\mathbf{y}, r)$

*University Osnabrück, Institute of Mathematics, torsten.goerner@uos.de

†University Chemnitz, Department of Mathematics, ralf.hielscher@mathematik.tu-chemnitz.de

‡University Osnabrück, Institute of Mathematics, and Helmholtz Zentrum München, Institute for Biomathematics and Biometry, stefan.kunis@math.uos.de

for a list of center points $\mathbf{y} \in Y$ and radii $r \in R$, we aim to reconstruct f from this data. Existence, uniqueness, and stability of this problem has been studied for the two dimensional case and for specific three dimensional geometries over the last decade, see e.g. [8, 3, 1, 15, 21] and references therein. Moreover, specific direct reconstruction algorithms for various geometries are discussed in [12, 19, 18, 11, 2, 7, 17, 9], variants for integrating detectors are discussed in [10, 5, 20, 26, 13, 25].

In this paper we consider the case of center points located at an arbitrary submanifold $Y \subset \mathbb{R}^d$. For this general case, explicit inversion formulae are not known and do not represent a realistic goal. Instead we focus on discretisations and fast algorithms for the forward problem such that the well developed machinery of iterative solvers can be applied, see [6] for a specific reconstruction algorithm. Our idea is to restrict the spherical mean value operator to periodic functions and to discretise these by trigonometric interpolation. In particular, this allows for error bounds that depend only on the function at hand. Moreover, we show that in the three dimensional case the discrete spherical mean value operator can be identified with a four-dimensional sparse Fourier transform with nodes and frequencies restricted to some three dimensional submanifolds. For this setting, the fast sparse Fourier transform [24, 16] applies and has the numerical complexity $\mathcal{O}(N^3 \log N)$, where N is the number of discretisation points in each dimension. This numerical complexity compares favorable to the numerical complexity of a finite element type discretisation which is $\mathcal{O}(N^5)$.

The structure of our paper is as follows. Section 2 defines the spherical mean value operator on the torus and proves in Theorem 2 a singular value decomposition in $L^2(\mathbb{T}^d)$. In Section 3, we define the discrete spherical mean value operator by trigonometric interpolation and prove associated error bounds in Theorem 4. The representation of the discrete operator as a four-dimensional Fourier transform can be found in Theorem 5 and Algorithm 2 is the corresponding fast scheme. In the last section we verify our theoretical findings numerically by considering a family of test functions with known spherical means and known Fourier coefficients. In particular, we show that our algorithms respect the theoretic error bounds and that they outperform the simplest finite element type discretisation with respect to computing time for large problem sizes.

2 The spherical mean value operator for periodic functions

We start by considering the spherical mean value operator on periodic functions and give its singular value decomposition in L^2. Let $d \in \mathbb{N}$, $\mathbf{x}, \mathbf{y} \in \mathbb{R}^d$, and denote by $\mathbf{x}\cdot\mathbf{y} := x_1y_1 + \ldots + x_dy_d$ and $|\mathbf{x}| := \sqrt{\mathbf{x}\cdot\mathbf{x}}$ the usual inner product and its induced norm, respectively. We define the d-dimensional torus $\mathbb{T}^d := \mathbb{R}^d/\mathbb{Z}^d = [-\frac{1}{2}, \frac{1}{2})^d$ and expand $f : \mathbb{T}^d \to \mathbb{R}$, $f \in L^2(\mathbb{T}^d)$, into its Fourier series

$$f(\mathbf{x}) = \sum_{\mathbf{z}\in\mathbb{Z}^d} \hat{f}_{\mathbf{z}} \mathrm{e}^{2\pi \mathrm{i}\, \mathbf{z}\cdot\mathbf{x}}$$

with Fourier coefficients $\hat{f}_{\mathbf{z}} \in \mathbb{C}$. Moreover, let $\mathbb{S}^{d-1} := \{\mathbf{x} \in \mathbb{R}^d : \mathbf{x} \cdot \mathbf{x} = 1\}$ be the unit sphere and denote $\mathrm{d}\sigma(\boldsymbol{\xi})$ its surface measure and

$$\omega_{d-1} := \int_{\mathbb{S}^{d-1}} 1 \,\mathrm{d}\sigma(\boldsymbol{\xi}) = \frac{2\pi^{\frac{d}{2}}}{\Gamma\left(\frac{d}{2}\right)},$$

its total area.

Lemma 1. *The spherical mean value operator*

$$\mathcal{M}\colon L^p(\mathbb{T}^d) \to L^p(\mathbb{T}^d \times [0,1],\, \mathrm{d}\mathbf{y} r^{d-1}\,\mathrm{d}r), \qquad \mathcal{M}f(\mathbf{y}, r) = \frac{1}{\omega_{d-1}} \int_{\mathbb{S}^{d-1}} f(\mathbf{y} + r\boldsymbol{\xi})\,\mathrm{d}\sigma(\boldsymbol{\xi})$$

satisfies $\|\mathcal{M}\|_\infty \leq 1$ *and* $\|\mathcal{M}\|_p^p \leq \frac{1}{d}$ *for* $1 \leq p < \infty$. *In particular, every* $f \in L^2(\mathbb{T}^d)$ *has mean values* $\mathcal{M}f \in L^2(\mathbb{T}^d \times [0,1],\, \mathrm{d}\mathbf{y} r^{d-1}\,\mathrm{d}r)$.

Proof. The assertion follows for $p = \infty$ right from the definition. For $1 \leq p < \infty$ we have

$$\|\mathcal{M}f\|_p^p \leq \int_0^1 \int_{\mathbb{T}^d} \frac{1}{\omega_{d-1}} \int_{\mathbb{S}^{d-1}} |f(\mathbf{y} + r\boldsymbol{\xi})|^p \,\mathrm{d}\boldsymbol{\xi}\,\mathrm{d}\mathbf{y} r^{d-1}\,\mathrm{d}r = \frac{1}{d}\,\|f\|_p^p\,.$$

□

For order $\nu \geq 0$ we define the Bessel functions $\mathcal{J}_\nu\colon \mathbb{R} \to \mathbb{R}$ by the integral representation (cf. [23, chap. 3.3])

$$\mathcal{J}_\nu(x) = \frac{x^\nu}{\Gamma\left(\nu + \frac{1}{2}\right)\Gamma\left(\frac{1}{2}\right)2^\nu} \int_0^\pi \mathrm{e}^{\mathrm{i}x\cos\xi}(\sin\xi)^{2\nu}\mathrm{d}\xi. \tag{1}$$

In the Hilbert space $L^2(\mathbb{T}^d)$ we have the following singular value decomposition of the spherical mean value operator.

Theorem 2. *For* $\mathbf{z} \in \mathbb{Z}^d$ *we define*

$$v_{\mathbf{z}}(\mathbf{x}) := \mathrm{e}^{2\pi\mathrm{i}\,\mathbf{z}\cdot\mathbf{x}}, \quad \tilde{u}_{\mathbf{z}}(\mathbf{y}, r) := \mathrm{e}^{2\pi\mathrm{i}\,\mathbf{z}\cdot\mathbf{y}} \frac{\Gamma\left(\frac{d}{2}\right)\mathcal{J}_{\frac{d-2}{2}}(2\pi\,|\mathbf{z}|\,r)}{(\pi\,|\mathbf{z}|\,r)^{\frac{d-2}{2}}}, \quad \lambda_{\mathbf{z}} := \|\tilde{u}_{\mathbf{z}}\|_2\,, \quad u_{\mathbf{z}} := \lambda_{\mathbf{z}}^{-1}\tilde{u}_{\mathbf{z}}.$$

Then $v_{\mathbf{z}}$, $\mathbf{z} \in \mathbb{Z}$, *is a complete orthonormal system in* $L^2(\mathbb{T}^d)$ *and* $u_{\mathbf{z}}$, $\mathbf{z} \in \mathbb{Z}$, *is an orthonormal system in* $L^2(\mathbb{T}^d \times [0,1],\, \mathrm{d}\mathbf{y} r^{d-1}\,\mathrm{d}r)$. *The spherical mean value operator has the singular value decomposition*

$$\mathcal{M}v_{\mathbf{z}} = \lambda_{\mathbf{z}} u_{\mathbf{z}}.$$

Moreover, there are constants $C_1, C_2 > 0$ *such that for all* $\mathbf{z} \in \mathbb{Z}^d$, $\mathbf{z} \neq \mathbf{0}$, *the estimate*

$$C_1\,|\mathbf{z}|^{\frac{1-d}{2}} \leq \lambda_{\mathbf{z}} \leq C_2\,|\mathbf{z}|^{\frac{1-d}{2}} \tag{2}$$

is valid.

Proof. For $\mathbf{z} \in \mathbb{Z}^d$ we have to compute

$$\mathcal{M}v_{\mathbf{z}}(\mathbf{y}, r) = \frac{1}{\omega_{d-1}} \int_{\mathbb{S}^{d-1}} \mathrm{e}^{2\pi \mathrm{i} \mathbf{z}\cdot(\mathbf{y}+r\boldsymbol{\xi})} \,\mathrm{d}\sigma(\boldsymbol{\xi}) = \mathrm{e}^{2\pi \mathrm{i}\, \mathbf{z}\cdot\mathbf{y}} \frac{1}{\omega_{d-1}} \int_{\mathbb{S}^{d-1}} \mathrm{e}^{2\pi\, \mathrm{i}\, r\, \boldsymbol{\xi}\cdot\mathbf{z}} \,\mathrm{d}\sigma(\boldsymbol{\xi}).$$

Let $\boldsymbol{\zeta} := \frac{\mathbf{z}}{|\mathbf{z}|}$. Then, using polar coordinates $\boldsymbol{\xi} = \sin\theta\, \boldsymbol{\eta} + \cos\theta\, \boldsymbol{\zeta}$, $\theta \in [0, \pi]$, $\boldsymbol{\eta} \perp \boldsymbol{\zeta}$, $|\boldsymbol{\eta}| = 1$, with respect to the north pole $\boldsymbol{\zeta} \in \mathbb{S}^{d-1}$, we can write the $d-1$ dimensional surface measure $\mathrm{d}\sigma(\boldsymbol{\xi}) = (\sin\theta)^{d-2} \,\mathrm{d}\tilde{\sigma}(\boldsymbol{\eta})\,\mathrm{d}\theta$ in terms of the $d-2$ dimensional surface measure $\mathrm{d}\tilde{\sigma}$. With the definition of the Bessel function (1), this yields

$$\begin{aligned}
\frac{1}{\omega_{d-1}} \int_{\mathbb{S}^{d-1}} \mathrm{e}^{2\pi\, \mathrm{i}\, r|\mathbf{z}|\, \boldsymbol{\xi}\cdot\boldsymbol{\zeta}} \,\mathrm{d}\sigma(\boldsymbol{\xi}) &= \frac{1}{\omega_{d-1}} \int_0^\pi \int_{\boldsymbol{\eta}\in\boldsymbol{\zeta}^\perp, |\boldsymbol{\eta}|=1} \mathrm{e}^{2\pi\, \mathrm{i}\, r|\mathbf{z}|\, \boldsymbol{\zeta}\cdot(\cos\theta\, \boldsymbol{\zeta} + \sin\theta\, \boldsymbol{\eta})} (\sin\theta)^{d-2} \,\mathrm{d}\tilde{\sigma}(\boldsymbol{\eta})\,\mathrm{d}\theta \\
&= \frac{\omega_{d-2}}{\omega_{d-1}} \int_0^\pi \mathrm{e}^{2\pi\, \mathrm{i}\, r|\mathbf{z}|\, \cos\theta} (\sin\theta)^{d-2} \,\mathrm{d}\theta \\
&= \frac{\pi^{-\frac{1}{2}} \Gamma\left(\frac{d}{2}\right)}{\Gamma\left(\frac{d-1}{2}\right)} \cdot \frac{\Gamma\left(\frac{d-1}{2}\right) \Gamma\left(\frac{1}{2}\right) \mathcal{J}_{\frac{d-2}{2}}(2\pi|\mathbf{z}|r)}{(\pi|\mathbf{z}|r)^{\frac{d-2}{2}}} \\
&= \Gamma(\tfrac{d}{2}) \cdot \frac{\mathcal{J}_{\frac{d-2}{2}}(2\pi\,|\mathbf{z}|\,r)}{(\pi\,|\mathbf{z}|\,r)^{\frac{d-2}{2}}}.
\end{aligned}$$

Since the system $\tilde{u}_{\mathbf{z}}$ is orthogonal in $L^2(\mathbb{T}^d \times [0,1], d\mathbf{y} r^{d-1}\,\mathrm{d}r)$ the singular value decomposition is shown.

Next we consider the singular values $\lambda_{\mathbf{z}}$, $\mathbf{z} \in \mathbb{Z}^d$,

$$\lambda_{\mathbf{z}}^2 = \|\tilde{u}_{\mathbf{z}}\|_2^2 = \frac{\left(\Gamma(\frac{d}{2})\right)^2}{\pi^{d-2}\,|\mathbf{z}|^d} \int_0^{|\mathbf{z}|} \mathcal{J}_{\frac{d-2}{2}}(2\pi r)^2 r \,\mathrm{d}r. \tag{3}$$

From the asymptotic expansion of the Bessel functions [23, Sec. 7.21] we know that there is a constant $C_3 > 0$ such that for all $r > 0$ we have

$$\left| \mathcal{J}_{\frac{d-2}{2}}(r) - \left(\frac{2}{\pi r}\right)^{1/2} \cos\left(r - \frac{d-3}{4}\pi\right) \right| \le C_3 r^{-3/2}. \tag{4}$$

Thus, the integral in (3) can be bounded by

$$\begin{aligned}
\int_0^{|\mathbf{z}|} \mathcal{J}_{\frac{d-2}{2}}(2\pi r)^2 r \,\mathrm{d}r &\le C_4 + \int_\varepsilon^{|\mathbf{z}|} \mathcal{J}_{\frac{d-2}{2}}(2\pi r)^2 r \,\mathrm{d}r \\
&\le C_4 + \int_\varepsilon^{|\mathbf{z}|} \frac{2}{\pi r} \cos(2\pi r - \tfrac{d-3}{4}\pi)^2 r \,\mathrm{d}r + C_5 \int_\varepsilon^{|\mathbf{z}|} r^{-3} r \,\mathrm{d}r \\
&\le C_4 + C_6\,|\mathbf{z}| + C_5 \varepsilon
\end{aligned}$$

which gives the upper bound. The lower bound follows analogously. □

3 Discretisation

Typically, the function $f : \mathbb{T}^d \to \mathbb{R}$ is given by discrete values $f(\mathbf{x_n})$ on a regular grid $\mathbf{x_n} \in X \subset \mathbb{T}^d$ and the spherical means $\mathcal{M}f(\mathbf{y}, r)$ have to be computed for scattered center points $\mathbf{y}$ and radii r. Subsequently, we suggest to compute an expansion into complex exponentials from the given data, then apply Theorem 2 which gives precise information about the spherical means of a complex exponential function, and finally perform an summation step to compute the spherical means of the complete expansion at the scattered center points.

We start by defining for some discretisation parameter $N \in 2\mathbb{N}$ the index sets

$$I_N := [0, N)^d \cap \mathbb{Z}^d, \quad J_N := \left[-\frac{N}{2}, \frac{N}{2}\right)^d \cap \mathbb{Z}^d,$$

and within the torus $\mathbb{T}^d = [-\frac{1}{2}, \frac{1}{2})^d$ the sampling grid

$$X := \{\mathbf{x_n} \in \mathbb{T}^d : \mathbf{x_n} = \left(\tfrac{2n_1+1-N}{2N}, \ldots, \tfrac{2n_d+1-N}{2N}\right), \mathbf{n} \in I_N\}.$$

Moreover, let T_N be the space of trigonometric polynomials $p : \mathbb{T}^d \to \mathbb{C}$,

$$p(\mathbf{x}) = \sum_{\mathbf{z} \in J_N} \hat{p}_{\mathbf{z}} \mathrm{e}^{2\pi \mathrm{i} \mathbf{z} \cdot \mathbf{x}},$$

and define the corresponding interpolation operator $\mathcal{I}_N : C(\mathbb{T}^d) \to T_N$, $f \mapsto \mathcal{I}_N f = p$,

$$p(\mathbf{x}) = f(\mathbf{x}), \quad \mathbf{x} \in X.$$

For subsequent use, we define the vector of samples $\mathbf{f} \in \mathbb{R}^{N^d}$, $\mathbf{f} := f(\mathbf{x_n})$, $\mathbf{x_n} \in X$. The Fourier coefficients of the trigonometric interpolation are given by

$$\hat{p}_{\mathbf{z}} = \frac{1}{N^d} \sum_{\mathbf{x} \in X} f(\mathbf{x}) \mathrm{e}^{-2\pi \mathrm{i} \mathbf{x} \cdot \mathbf{z}}, \quad \mathbf{z} \in J_N, \tag{5}$$

and can be computed from the samples by means of the fast Fourier transform (FFT). Moreover, sufficiently smooth functions $f(\mathbf{x}) = \sum_{\mathbf{k} \in \mathbb{Z}} \hat{f}_{\mathbf{z}} \mathrm{e}^{2\pi \mathrm{i} \mathbf{z} \cdot \mathbf{x}}$ allow for a simple bound on the interpolation error

$$\|f - \mathcal{I}_N f\|_\infty \leq 2 \sum_{\mathbf{z} \in \mathbb{Z}^d \setminus J_N} \left|\hat{f}_{\mathbf{z}}\right|. \tag{6}$$

Remark 3. The trigonometric polynomial p interpolates on the symmetric spatial grid $X \subset \mathbb{T}^d$ with an even discretisation number $N \in 2\mathbb{N}$. For real interpolation values, the computed polynomial is nevertheless complex valued in general but can be modified to a real valued trigonometric polynomial interpolating the data by extending its Fourier coefficients to $[-\frac{N}{2}, \frac{N}{2}]^d \cap \mathbb{Z}^d \supset J_N$ appropriately.

Instead of the trigonometric interpolant we will also use the Fourier partial sum, defined by

$$\mathcal{S}_N f(\mathbf{x}) = \sum_{\mathbf{z}\in J_N} \hat{f}_{\mathbf{z}} \mathrm{e}^{2\pi \mathrm{i}\mathbf{z}\cdot\mathbf{x}}.$$

Since one is not able to compute the required coefficients only from the given function samples, this variant is only useful for theoretical purposes but it gives us also a higher capability to compare the theoretical with the numerical results.

In order to give upper bounds for the resulting errors of our discretisation of the spherical mean value operator we introduce for $s > 0$ the Sobolev space $\mathcal{H}_s(\mathbb{T}^d) \subset L^2(\mathbb{T}^d)$ as the subspace of all functions $f \in L^2(\mathbb{T}^d)$ with finite Sobolev norm

$$\|f\|_s^2 = \sum_{\mathbf{z}\in\mathbb{Z}^d} |\hat{f}_{\mathbf{z}}|^2 \left(1 + (2\pi)^2 |\mathbf{z}|^2\right)^s.$$

For those functions we have the following result.

Theorem 4. *Let $d \in \mathbb{N}$, $N \in 2\mathbb{N}$, $N \geq 4\sqrt{d}$, $f \in \mathcal{H}_s(\mathbb{T}^d)$, $\mathbf{y} \in \mathbb{T}^d$, and $r \in (0, 1]$ be given. Then for $s > \frac{d}{2}$ the error can be bounded by*

$$|\mathcal{M}f(\mathbf{y}, r) - \mathcal{M}\mathcal{I}_N f(\mathbf{y}, r)| \leq \frac{2^{s-\frac{d}{2}+1} \cdot \pi^{-s+\frac{d}{4}}}{\sqrt{\Gamma\left(\frac{d}{2}\right) \cdot (d - 2s)}} \|f\|_s N^{-s+\frac{d}{2}}.$$

Moreover, it exists a constant $C(f, s, d, r) > 0$ such that for $s > \frac{1}{2}$ the estimate

$$|\mathcal{M}f(\mathbf{y}, r) - \mathcal{M}\mathcal{S}_N f(\mathbf{y}, r)| \leq \sqrt{\frac{\Gamma\left(\frac{d}{2}\right)}{2s-1}} \frac{2^{s+\frac{d}{2}-1}}{\pi^{s+\frac{d}{4}} r^{\frac{d-1}{2}}} \|f\|_s N^{-s+\frac{1}{2}} + C(f, s, d, r) N^{-s-\frac{1}{2}}$$

is valid.

Proof. Since f is continuous, Lemma 1, Equation (6), the Cauchy–Schwarz inequality, and the auxiliary estimate

$$\left(1 + (2\pi)^2 |\mathbf{z}|^2\right)^{-s} \leq \int_{\Omega(\mathbf{z})} \left(1 + (2\pi)^2 (|\mathbf{x}| - \sqrt{d})^2\right)^{-s} \mathrm{d}\mathbf{x}, \quad \Omega(\mathbf{z}) = \times_{j=1}^d [|z_j|, |z_j| + 1],$$

lead to

$$\begin{aligned}
|\mathcal{M}f(\mathbf{y},r) - \mathcal{M}\mathcal{I}_N f(\mathbf{y},r)|^2 &\leq \|\mathcal{M}\|_\infty^2 \, \|f - \mathcal{I}_N f\|_\infty^2 \\
&\leq 4 \left(\sum_{\mathbf{z}\in\mathbb{Z}^d\setminus J_N} \left|\hat{f}_\mathbf{z}\right| (1+(2\pi)^2 |\mathbf{z}|^2)^{\frac{s}{2}} (1+(2\pi)^2|\mathbf{z}|^2)^{-\frac{s}{2}} \right)^2 \\
&\leq 4 \|f\|_s^2 \sum_{\substack{\mathbf{z}\in\mathbb{Z}^d \\ |\mathbf{z}|\geq \frac{N}{2}}} \left(1+(2\pi)^2|\mathbf{z}|^2\right)^{-s} \\
&\leq 4 \|f\|_s^2 \int\limits_{|\mathbf{z}|\geq\frac{N}{2}} (1+(2\pi)^2(|\mathbf{z}|-\sqrt{d})^2)^{-s} \, \mathrm{d}\mathbf{z} \\
&= 4\omega_{d-1} \|f\|_s^2 \int\limits_{\frac{N}{2}-\sqrt{d}}^{\infty} (1+(2\pi)^2 r^2)^{-s} (r+\sqrt{d})^{d-1} \, \mathrm{d}r.
\end{aligned}$$

The assumption $N \geq 4\sqrt{d}$ implies $N/2 - \sqrt{d} \geq N/4$. Using $r + \sqrt{d} \leq 2r$, due to $r \geq \frac{N}{2} - \sqrt{d} \geq \frac{N}{4} \geq \sqrt{d}$, and the inequality $(2\pi)^2 r^2 + 1 \geq (2\pi)^2 r^2$, we obtain

$$|\mathcal{M}f(\mathbf{y},r) - \mathcal{M}\mathcal{I}_N f(\mathbf{y},r)|^2 \leq 4\omega_{d-1} \|f\|_s^2 (2\pi)^{-2s} 2^{d-1} \int\limits_{\frac{N}{4}}^{\infty} r^{-2s+d-1} \mathrm{d}r$$

and because of $2s - d + 1 > 1$ direct calculation shows the first assertion. With Equation (4) the Bessel function can be bounded by

$$\left| \mathcal{J}_{\frac{d-2}{2}}(2\pi|\mathbf{z}|r) \right| \leq \sqrt{\frac{1}{|\mathbf{z}|\pi^2 r}} + C_1(d,r)|\mathbf{z}|^{-\frac{3}{2}}, \quad C_1(d,r) > 0.$$

Thus, with $v_\mathbf{z}(\mathbf{x}) = \mathrm{e}^{2\pi \mathrm{i}\mathbf{z}\cdot\mathbf{x}}$ we obtain the estimate

$$\begin{aligned}
|\mathcal{M}f(\mathbf{y},r) - \mathcal{M}\mathcal{S}_N f(\mathbf{y},r)| &\leq \left| \sum_{\mathbf{z}\in\mathbb{Z}^d\setminus J_N} \hat{f}_\mathbf{z} \left(\mathcal{M}v_\mathbf{z}\right)(\mathbf{y},r) \right| = \left| \sum_{\mathbf{z}\in\mathbb{Z}^d\setminus J_N} \hat{f}_\mathbf{z} \frac{\Gamma\left(\frac{d}{2}\right) \mathcal{J}_{\frac{d-2}{2}}(2\pi|\mathbf{z}|r)}{(\pi|\mathbf{z}|r)^{\frac{d-2}{2}}} \right| \\
&\leq \frac{\Gamma\left(\frac{d}{2}\right)}{\pi^{\frac{d}{2}} r^{\frac{d-1}{2}}} \sum_{\mathbf{z}\in\mathbb{Z}^d\setminus J_N} \left|\hat{f}_\mathbf{z}\right| \left(|\mathbf{z}|^{\frac{1-d}{2}} + C_2(d,r)|\mathbf{z}|^{-\frac{1+d}{2}} \right).
\end{aligned}$$

and with the method of the first part of the proof we get the second assertion. For example the

first sum yields

$$\sum_{\mathbf{z}\in J_N} \left|\hat{f}_{\mathbf{z}}\right| |\mathbf{z}|^{\frac{1-d}{2}} \leq (2\pi)^{-s} \sum_{\mathbf{z}\in\mathbb{Z}^d\setminus J_N} \left|\hat{f}_{\mathbf{z}}\right| \left(1+(2\pi)^2|\mathbf{z}|^2\right)^{\frac{s}{2}} |\mathbf{z}|^{\frac{1-d}{2}-s}$$

$$\leq (2\pi)^{-s} \|f\|_s \left(\sum_{\mathbf{z}\in\mathbb{Z}^d\setminus J_N} |\mathbf{z}|^{1-d-2s}\right)^{\frac{1}{2}} \leq \frac{\omega_{d-1}\cdot 2^{d-1}}{(2\pi)^s} \|f\|_s \int_{\frac{N}{4}}^{\infty} r^{-2s}\mathrm{d}r.$$

□

Next, we are concerned with the numerical implementation of the discrete spherical mean values $\mathcal{MI}_N f(\mathbf{y}_{m_1}, r_{m_2})$, $\mathbf{y}_{m_1} \in \mathbb{T}^d$, $m_1 = 1,\dots,M_1$, $r_{m_2} \in [0,1]$, $m_2 = 1,\dots,M_2$. Our first algorithm we derive straight forward from Theorem 2. We start by computing the Fourier coefficients

$$\hat{p}_{\mathbf{z}} = \frac{1}{N^d} \cdot \sum_{\mathbf{x}\in X} f(\mathbf{x}) \mathrm{e}^{-2\pi \mathrm{i}\mathbf{z}\cdot\mathbf{x}}, \quad \mathbf{z}\in J_N,$$

of the trigonometric interpolant $\mathcal{I}_N f$ by a fast Fourier transform. The numerical complexity of this first step is $\mathcal{O}(N^d \log N)$. In the second step we compute the Fourier coefficients $\tilde{h}_{\mathbf{z},m_2}$,

$$\tilde{h}_{\mathbf{z},m_2} := \hat{p}_{\mathbf{z}} \cdot \frac{\Gamma\left(\frac{d}{2}\right) \mathcal{J}_{\frac{d-2}{2}}(2\pi\,|\mathbf{z}|\,r_{m_2})}{(\pi\,|\mathbf{z}|\,r_{m_2})^{\frac{d-2}{2}}}, \quad \mathbf{z}\in J_N,$$

of $\mathcal{MI}_N f(\cdot, r_{m_2})$ for every fixed radius r_{m_2}, $m_2 = 1,\dots,M_2$. This step has the numerical complexity $\mathcal{O}(M_2 N^d)$. In the last step we compute the spherical means

$$\mathcal{MI}_N f(\mathbf{y}_{m_1}, r_{m_2}) = \sum_{\mathbf{z}\in J_N} \tilde{h}_{\mathbf{z},m_2} \mathrm{e}^{2\pi\mathrm{i}\mathbf{z}\cdot\mathbf{y}_{m_1}}, \quad m_1 = 1,\dots,M_1$$

for every fixed radius r_{m_2} by a nonequispaced fast Fourier transform (NFFT, [14]), which has the total numerical complexity $\mathcal{O}(M_2(N^d\log N + M_1))$. An description of our algorithm in pseudocode is given in Algorithm 1. For the typical case that the center points are located at a N^{d-1}–dimensional submanifold of the torus $\mathbb{T}^d$ we may assume $M_1 = \mathcal{O}(N^{d-1})$ and $M_2 = \mathcal{O}(N)$. In this case our algorithm has the numerical complexity $\mathcal{O}(N^4 \log N)$ which compares favorable to the numerical complexity $O(N^{2d-1})$ of a naive implementation whenever $d > 2$.

Let us now consider the practical important case $d = 3$. Then the discrete spherical mean value operator can be written in terms of a sparse four-dimensional Fourier transform. More precisely we have the following result.

Theorem 5. *For the three dimensional index set $J_N \subset \mathbb{Z}^3$ we denote by*

$$\tilde{J}_N := \left\{(\mathbf{z},\zeta) \in J_N \times \left[-\frac{\sqrt{3}N}{2}, \frac{\sqrt{3}N}{2}\right] : |\zeta| = |\mathbf{z}|\right\} \setminus \{\mathbf{0}\} \tag{7}$$

Algorithm 1 Discrete spherical mean value operator

Input

$d \in \mathbb{N}$ ▷ spatial dimension

$N \in 2\mathbb{N}$, $M_1 \in \mathbb{N}$, $M_2 \in \mathbb{N}$ ▷ discretisation parameter

$\mathbf{f} \in \mathbb{R}^{N^d}$ ▷ samples

$\mathbf{y}_{m_1} \in \mathbb{T}^d : m_1 = 1, \dots, M_1 - 1$ ▷ center points

$r_{m_2} \in [0,1], m_2 = 1, \dots, M_2 - 1$ ▷ radii

Output

$\mathbf{g} \in \mathbb{C}^{M_1 M_2}$ ▷ spherical mean values

for $\mathbf{z} \in J_N$ **do**

  $\hat{p}_{\mathbf{z}} = \frac{1}{N^d} \sum_{\mathbf{x} \in X} f(\mathbf{x}) \mathrm{e}^{-2\pi \mathrm{i} \mathbf{z} \cdot \mathbf{x}}$ ▷ DFT, Eq. (5)

end for

for $m_2 = 1, ..., M_2$ **do**

  for $\mathbf{z} \in J_N \setminus \{\mathbf{0}\}$ **do**

    $\tilde{h}_{\mathbf{z},m_2} = \hat{p}_{\mathbf{z}} \cdot \frac{\Gamma\left(\frac{d}{2}\right) \mathcal{J}_{\frac{d-2}{2}}(2\pi|\mathbf{z}|r_{m_2})}{(\pi|\mathbf{z}|r_{m_2})^{\frac{d-2}{2}}}$ ▷ multiplier

  end for

  $\tilde{h}_{\mathbf{0},m_2} := \hat{f}_{\mathbf{0}}$

  for $m_1 = 1, \dots, M_1$ **do**

    $g_{m_1,m_2} := \sum_{\mathbf{z} \in J_N} \tilde{h}_{\mathbf{z},m_2} \mathrm{e}^{2\pi \mathrm{i} \mathbf{z} \cdot \mathbf{y}_{m_1}}$ ▷ NDFT

  end for

end for

the corresponding double cone in $\mathbb{R}^4$. Let, $\hat{p}_{\mathbf{z}}$ be the Fourier coefficients of the trigonometric interpolant $\mathcal{I}_N f$ and let

$$\hat{h}_{\mathbf{z},\zeta} := \frac{\hat{p}_{\mathbf{z}}}{\zeta}, \quad (\mathbf{z},\zeta) \in \tilde{J}_N, \tag{8}$$

be the corresponding Fourier coefficients supported on the cone $\tilde{J}_N$. Then the spherical mean value operator has the representation

$$\mathcal{M}\mathcal{I}_N f(\mathbf{y},r) = \hat{p}_{\mathbf{0}} - \frac{\mathrm{i}}{4\pi r} \sum_{(\mathbf{z},\zeta)\in\tilde{J}_N} \hat{h}_{\mathbf{z},\zeta} \cdot \mathrm{e}^{2\pi\mathrm{i}(\mathbf{z},\zeta)\cdot(\mathbf{y},r)}. \tag{9}$$

Proof. First of all we observe that for all $\mathbf{z} \in J_N\backslash\{\mathbf{0}\}$ and $r > 0$

$$\frac{\Gamma\left(\frac{3}{2}\right)\mathcal{J}_{\frac{1}{2}}(2\pi\,|\mathbf{z}|\,r)}{\sqrt{\pi\,|\mathbf{z}|\,r}} = \frac{\sin 2\pi\,|\mathbf{z}|\,r}{2\pi\,|\mathbf{z}|\,r} = \frac{-\mathrm{i}}{4\pi\,|\mathbf{z}|\,r}\left(\mathrm{e}^{2\pi\mathrm{i}|\mathbf{z}|r} - \mathrm{e}^{-2\pi\mathrm{i}|\mathbf{z}|r}\right). \tag{10}$$

Hence, we have by Theorem 2

$$\begin{aligned}
\mathcal{M}\mathcal{I}_N f(\mathbf{y},r) &= \sum_{\mathbf{z}\in J_N} \hat{p}_{\mathbf{z}} \cdot \left(\mathcal{M}\mathrm{e}^{2\pi\mathrm{i}\mathbf{z}\cdot(\cdot)}\right)(\mathbf{y},r) \\
&= \hat{p}_{\mathbf{0}} + \sum_{\mathbf{z}\in J_N\backslash\{\mathbf{0}\}} \hat{p}_{\mathbf{z}} \cdot \mathrm{e}^{2\pi\mathrm{i}\mathbf{z}\cdot\mathbf{y}} \cdot \frac{\Gamma\left(\frac{3}{2}\right)\mathcal{J}_{\frac{1}{2}}(2\pi\,|\mathbf{z}|\,r)}{\sqrt{\pi\,|\mathbf{z}|\,r}} \\
&= \hat{p}_{\mathbf{0}} + \frac{-\mathrm{i}}{4\pi r} \cdot \sum_{\mathbf{z}\in J_N\backslash\{\mathbf{0}\}} \frac{\hat{p}_{\mathbf{z}}}{|\mathbf{z}|} \cdot \mathrm{e}^{2\pi\mathrm{i}\mathbf{z}\cdot\mathbf{y}} \cdot \left(\mathrm{e}^{2\pi\mathrm{i}|\mathbf{z}|r} - \mathrm{e}^{-2\pi\mathrm{i}|\mathbf{z}|r}\right).
\end{aligned}$$

Defining the coefficients $\hat{h}_{\mathbf{z},\zeta}$ as in (8) we arrive at

$$\mathcal{M}\mathcal{I}_N f(\mathbf{y},r) = \hat{p}_{\mathbf{0}} - \frac{\mathrm{i}}{4\pi r} \cdot \sum_{(\mathbf{z},\zeta)\in\tilde{J}_N} \hat{h}_{\mathbf{z},\zeta} \cdot \mathrm{e}^{2\pi\mathrm{i}(\mathbf{z},\zeta)\cdot(\mathbf{y},r)}.$$

□

With the assumption that the center points $\mathbf{y}_{m_1}$, $m_1 = 1,\ldots,M_1$, are located on a smooth two dimensional submanifold of $\mathbb{T}^3$ the sum in (9) is in fact a sparse four-dimensional Fourier transform with frequencies $(\mathbf{z},\zeta) \in \tilde{J}_N$ and sampling points $(\mathbf{y}_{m_1}, r_{m_2})$, $m_1 = 1,\ldots,M_1$, $m_2 = 1,\ldots,M_2$. Each set is supported on a smooth three dimensional submanifolds of $\mathbb{R}^4$. If moreover $M_1 = \mathcal{O}(N^2)$ and $M_2 = \mathcal{O}(N)$, such a sparse Fourier transform can be efficiently computed by means of the butterfly algorithm [24, 16] resulting in an algorithm with numerical complexity $\mathcal{O}(N^3 \log N)$. A pseudocode description for computing the discrete spherical mean values by this approach is given in Algorithm 2. A comparison between the complexities of the algorithms can be found in Table 1.

Algorithm 2 Discrete spherical mean value operator, using sparse FFT, $d = 3$

Input and **Output** as in Algorithm 1

for $\mathbf{z} \in J_N$ **do**
  $\hat{p}_{\mathbf{z}} = \frac{1}{N^3} \sum_{\mathbf{x} \in X} f(\mathbf{x}) \mathrm{e}^{-2\pi \mathrm{i} \mathbf{z} \cdot \mathbf{x}}$ ▷ DFT, Eq. (5)
end for
for $(\mathbf{z}, \zeta) \in \tilde{J}_N$ **do**
  $\hat{h}_{\mathbf{z},\zeta} := \frac{\hat{p}_{\mathbf{z}}}{\zeta}$ ▷ coefficients for sparse FFT, Eq. (8)
end for
for $m_1 = 1, \ldots, M_1$ **do**
  for $m_2 = 1, \ldots, M_2$ **do**
    $g_{m_1,m_2} = \hat{p}_{\mathbf{0}} - \frac{\mathrm{i}}{4\pi r} \sum_{(\mathbf{z},\zeta) \in \tilde{J}_N} \hat{h}_{\mathbf{z},\zeta} \cdot \mathrm{e}^{2\pi \mathrm{i} (\mathbf{z},\zeta) \cdot (\mathbf{y}_{m_1}, r_{m_2})}$ ▷ sparse FFT, Eq. (9)
  end for
end for

	$d = 2$	$d = 3$
Input and output data	$\mathcal{O}(N^2)$	$\mathcal{O}(N^3)$
Algorithm	arithmetic operations	
Naive implementation, Alg. 3	$\mathcal{O}(N^3)$	$\mathcal{O}(N^5)$
Fourier method, using NFFT, Alg. 1	$\mathcal{O}(N^3 \log N)$	$\mathcal{O}(N^4 \log N)$
Fourier method, using sparse FFT, Alg. 2	–	$\mathcal{O}(N^3 \log N)$

Table 1: Complexities of the algorithms for spatial dimensions $d = 2$ and $d = 3$.

Remark 6. In order to apply the above algorithms to compactly supported functions $f \in C(\mathbb{R}^d)$. We assume $\operatorname{supp} f \subset \left\{\mathbf{x} \in \mathbb{R}^d : |\mathbf{x}| \leq R\right\}, R \in (0, 0.5)$, and define the periodised function $\tilde{f}$ by

$$\tilde{f}(\mathbf{x}) := \sum_{\mathbf{z} \in \mathbb{Z}^d} f(\mathbf{x} + \mathbf{z}).$$

Then $r \leq 1 - R - |\mathbf{y}|$ is a sufficient condition on the support of f, the location of the center points $\mathbf{y}$ and the radii r such that the spherical means $\mathcal{M}f(\mathbf{y}, r)$ of the compactly supported function f and the spherical means $\mathcal{M}\tilde{f}(\mathbf{y}, r)$ of the periodic function $\tilde{f}$ agree.

4 Numerical Experiments

In this section, we analyse numerical results of the presented discretisations of the spherical mean value operator. In particular, we consider the approximation errors and the running times. The algorithms are implemented in Matlab and the numerical results were obtained on an Intel Core i7 CPU 920 with 2.66 GHz and 12 GByte RAM running OpenSUSE Linux 11.1 X86-64 and Matlab R2010a.

Let us start by defining some test functions. Let a size parameter $t \in [0, 0.5]$, a smoothness parameter $s \in \mathbb{N}_0$, and the radial test function $f_{d,s,t} : \mathbb{R}^d \to \mathbb{R}_+$,

$$f_{d,s,t}(\mathbf{x}) := \begin{cases} \varphi_{s,t}\left(|\mathbf{x}|^2\right) & |\mathbf{x}| \leq t, \\ 0 & \text{otherwise,} \end{cases} \qquad \varphi_{s,t}(\tau) := \left(1 - \frac{\tau}{t^2}\right)^s, \tag{11}$$

be given. We compute spherical means of these test functions analytically by using the following statement for radial functions.

Lemma 7. *Let a spatial dimension $d \in \mathbb{N}$, $d \geq 2$, a center point $\mathbf{y} \in \mathbb{R}^d$, a radius $r \geq 0$, and a radial function $f : \mathbb{R}^d \to \mathbb{R}$, $f(\mathbf{x}) = \varphi\left(|\mathbf{x}|^2\right)$ for some function $\varphi\colon [0, \infty) \to \mathbb{R}$, be given. Then the spherical mean values of the function f can be computed by*

$$\mathcal{M}f(\mathbf{y}, r) = \frac{\omega_{d-2}}{\omega_{d-1}} \int_{-1}^{1} \varphi\left(|\mathbf{y}|^2 + r^2 + 2r|\mathbf{y}|\tau\right) (1 - \tau^2)^{\frac{d-3}{2}} \mathrm{d}\tau.$$

Proof. First we assume without loss of generality that $\mathbf{y} = |\mathbf{y}|\, \mathbf{e}_d$, where $\mathbf{e}_d = (0, \ldots, 0, 1)^\top \in \mathbb{R}^d$. Then

$$\begin{aligned} \mathcal{M}f(\mathbf{y}, r) &= \frac{1}{\omega_{d-1}} \int_{\mathbb{S}^{d-1}} \varphi\left(|\mathbf{y} + r\boldsymbol{\xi}|^2\right) \mathrm{d}\sigma(\boldsymbol{\xi}) \\ &= \frac{1}{\omega_{d-1}} \int_{\mathbb{S}^{d-1}} \varphi\left(|\mathbf{y}|^2 + r^2 + 2r\,|\mathbf{y}|\,\boldsymbol{\xi} \cdot \mathbf{e}_d\right) \mathrm{d}\sigma(\boldsymbol{\xi}) \\ &= \frac{1}{\omega_{d-1}} \int_{-1}^{1} \int_{\mathbb{S}^{d-2}} \varphi\left(|\mathbf{y}|^2 + r^2 + 2r|\mathbf{y}|\tau\right) \mathrm{d}\sigma(\tilde{\boldsymbol{\xi}}) (1 - \tau^2)^{\frac{d-3}{2}}\, \mathrm{d}\tau. \end{aligned}$$

□

Next we use the above lemma to compute the spherical mean value operator of some of the test functions (11) explicitly.

Example 8. Let us start with spatial dimension $d = 2$. Then we have

$$\mathcal{M}f_{s,t}(\mathbf{y}, r) = \frac{1}{\pi} \int_0^{\vartheta_0} \varphi_{s,t}\left(|\mathbf{y}|^2 + r^2 - 2r|\mathbf{y}| \cos\vartheta\right) \mathrm{d}\vartheta,$$

where

$$\vartheta_0 := \vartheta_0\left(|\mathbf{y}|, r, t\right) := \begin{cases} \pi & \text{for} \quad t^2 \geq (|\mathbf{y}| + r)^2, \\ 0 & \text{for} \quad t^2 < (|\mathbf{y}| - r)^2, \\ \arccos \frac{|\mathbf{y}|^2 + r^2 - t^2}{2r|\mathbf{y}|} & \text{else.} \end{cases}$$

Fixing the smoothness parameter $s \in \mathbb{N}_0$ gives an explicit solution of the integral. With adequate coefficients $b_{s,k} := b_{s,k}(\mathbf{y}, r, t) \in \mathbb{R}$, $k \in \{0, 1, \ldots, s\}$, we have

$$\varphi_{s,t}\left(|\mathbf{y}|^2 + r^2 - 2r|\mathbf{y}| \cos\vartheta\right) = \sum_{k=0}^{s} b_{s,k} (\cos\vartheta)^k$$

and it follows

$$\mathcal{M}f_{s,t}(\mathbf{y}, r) = \frac{1}{\pi} \sum_{k=0}^{s} b_{s,k} \int_0^{\vartheta_0} (\cos\vartheta)^k \mathrm{d}\vartheta.$$

For example $s = 0$ yields the coefficient $b_{0,0} = 1$ and $s = 1$ yields the coefficients $b_{1,0} = \frac{t^2 - |\mathbf{y}|^2 - r^2}{t^2}$ and $b_{1,1} = \frac{2r|\mathbf{y}|}{t^2}$. Hence, we obtain

$$\mathcal{M}f_{2,0,t}(\mathbf{y}, r) = \frac{\vartheta_0}{\pi} \quad \text{and}$$

$$\mathcal{M}f_{2,1,t}(\mathbf{y}, r) = \frac{1}{\pi}\left(b_{1,0} \cdot \vartheta_0 + b_{1,1} \cdot \sin\vartheta_0\right) = \frac{\vartheta_0 \cdot (t^2 - |\mathbf{y}|^2 - r^2) + 2r|\mathbf{y}| \sin\vartheta_0}{\pi t^2}.$$

Example 9. Since the weight disappears for dimension $d = 3$ we define a primitive $\Phi_{s,t} : \mathbb{R} \to \mathbb{R}$ of $\varphi_{s,t}$ and an auxiliary quantity $\tau_0 \in \mathbb{R}_+$,

$$\Phi_{s,t}(\tau) := -\frac{(t^2 - \tau)^{s+1}}{t^{2s}\,(1+s)}, \quad \tau_0 := \begin{cases} (|\mathbf{y}| + r)^2 & \text{for} \quad t^2 \geq (|\mathbf{y}| + r)^2, \\ (|\mathbf{y}| - r)^2 & \text{for} \quad t^2 < (|\mathbf{y}| - r)^2, \\ t^2 & \text{else,} \end{cases}$$

and obtain for $\mathbf{y} \neq \mathbf{0}$ and $r \neq 0$ the closed-form expression

$$\mathcal{M}f_{3,s,t}(\mathbf{y}, r) = \frac{1}{4r|\mathbf{y}|} \cdot \left(\Phi_{s,t}(\tau_0) - \Phi_{s,t}\left((|\mathbf{y}| - r)^2\right)\right).$$

For example with parameters $s = 0$ and $s = 1$ we get the formulas

$$\mathcal{M}f_{3,0,t} = \frac{\tau_0 - (|\mathbf{y}| - r)^2}{4r|\mathbf{y}|}, \quad \mathcal{M}f_{3,1,t} = \frac{\left(t^2 - (|\mathbf{y}| - r)^2\right)^2 - (t^2 - \tau_0)^2}{8r|\mathbf{y}|t^2}.$$

Moreover, Sonine's integral [23, Chapter 12.11] yields the Fourier transform of these test functions

$$\hat{f}_{d,s,t}(\mathbf{z}) = \frac{\Gamma(s+1)t^{\frac{d}{2}-s}}{\pi^s} \cdot \frac{\mathcal{J}_{s+\frac{d}{2}}(2\pi\,|\mathbf{z}|\,t)}{|\mathbf{z}|^{s+\frac{d}{2}}}, \tag{12}$$

which, in conjunction with [23, Sec. 7.21], allows for the estimate

$$\left|\hat{f}_{d,s,t}(\mathbf{z})\right| \leq C_{d,s,t} \cdot (1+|\mathbf{z}|^2)^{-\frac{1}{2}\left(s+\frac{d+1}{2}\right)}. \tag{13}$$

and thus $f_{d,s,t} \in \mathcal{H}_{s+\frac{1}{2}-\varepsilon}(\mathbb{T}^d)$ for every $\varepsilon > 0$. Theorem 4 implies

$$\begin{aligned} &|\mathcal{M}f_{d,s,t}(\mathbf{y},r) - \mathcal{M}\mathcal{I}_N f_{d,s,t}(\mathbf{y},r)| \leq C_{d,s,t,f,\varepsilon} \cdot N^{\frac{d}{2}-s-\frac{1}{2}+\varepsilon} \quad \text{and} \\ &|\mathcal{M}f_{d,s,t}(\mathbf{y},r) - \mathcal{M}\mathcal{S}_N f_{d,s,t}(\mathbf{y},r)| \leq C_{d,s,t,f,\varepsilon} \cdot N^{-s+\varepsilon}. \end{aligned}$$

Additionally to the two Algorithms 1 and 2 for the discrete spherical mean value operator we consider also a variant that makes use of the exact Fourier coefficients (12) of our test functions and implements $\mathcal{M}S_N f$. This algorithm is labeled as Algorithm 1a in the following tables and figures. We compare our algorithm for the computation of the spherical mean value operator also to a naive implementation which is based on a simple interpolation of the function f by piecewise constant functions and a simple quadrature rule, see Algorithm 3.

Algorithm 3 Discrete spherical mean value operator, ad-hoc scheme, $d = 2$

Input and **Output** as in Algorithm 1

for $m_2 = 1, ..., M_2$ **do**
  $n := \lceil 2\pi r_{m_2} N \rceil$ ▷ number of sampling points
  for $m_1 = 1, ..., M_1$ **do**
    $s := 0$
    for $l = 0, ..., n-1$ **do**
      $\varphi_l := \frac{2\pi l}{n}$
      $\mathbf{x}_l := \mathbf{y}_{m_1} + r_{m_2} \begin{pmatrix} \cos\varphi_l \\ \sin\varphi_l \end{pmatrix}$ ▷ sampling point
      $\widetilde{\mathbf{x}}_l := \left(\frac{2\left[(\mathbf{x}_l)_1 \cdot N + \frac{N}{2} - \frac{1}{2}\right] + 1 - N}{2N}, \frac{2\left[(\mathbf{x}_l)_2 \cdot N + \frac{N}{2} - \frac{1}{2}\right] + 1 - N}{2N} \right)^\top$ ▷ nearest grid point
      $s := s + f\left(\widetilde{\mathbf{x}}_l\right)$
    end for
    $g_{m1,m2} := \frac{1}{n} \cdot s$
  end for
end for

We compare the approximation error with respect to the discretisation parameter N of the quadrature based Algorithm 3 and the Fourier based Algorithm 1 and its variant 1a. Therefore,

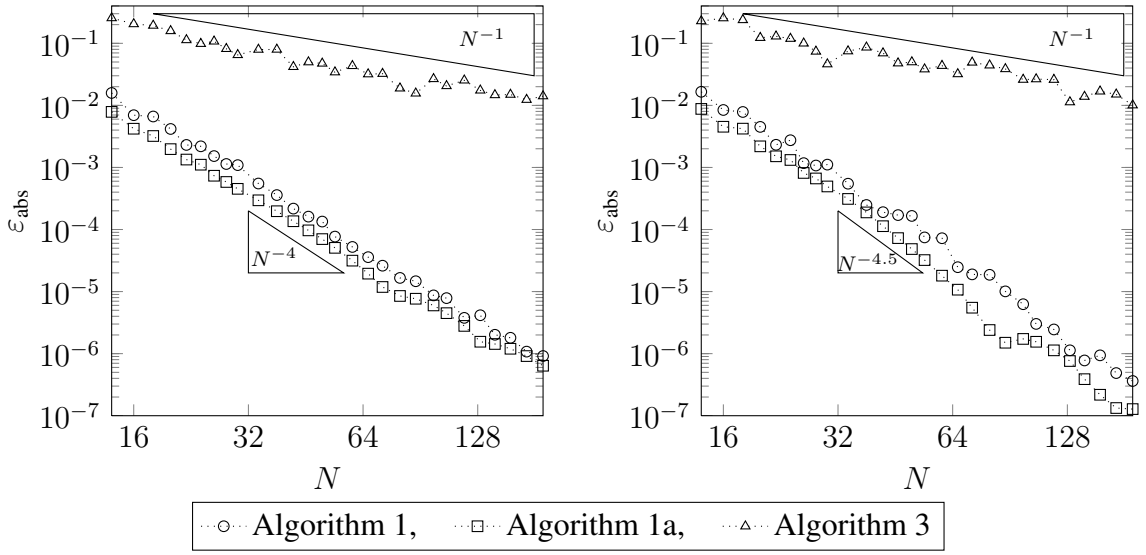

Figure 1: Accuracy with respect to the discretisation parameter N for spatial dimension $d = 2$ (left) and $d = 3$ (right), and test functions with smoothness parameter $s = 3$.

we fix the test function $f_{s,t,d}$ with smoothness parameter $s = 3$, size parameter $t = \frac{1}{5}$, and dimension $d = 2, 3$ and plot the maximum error

$$\varepsilon_{\text{abs}} = \max_{\substack{\mathbf{y}\in\mathbb{T}^d \\ r\in[0,1]}} \left|\left(\mathcal{M}f_{d,s,t}\right)(\mathbf{y}, r) - g(\mathbf{y}, r)\right|,$$

where $g(\mathbf{y}, r)$ is the result of one of the algorithms. The results are plotted in Figure 1 which clearly confirms the superior error rate of the Fourier based discretisation compared to the discretisation by piecewise constant functions. Table 2 summarises the numerical and theoretical convergence rates with respect to the smoothness parameter s. This indicates that the convergence rate of the Fourier based algorithms for the considered test functions is even better than the theoretical bound proven in Theorem 4. We suspect that this is related to the fact, that the Fourier coefficients of $f_{s,t,d}$ oscillate.

	$d=2$			$d=3$		
s	Alg. 3	Alg. 1	Alg. 1a	Alg. 3	Alg. 1	Alg. 1a
0	0.74	0.73	0.71	1.10	1.12	1.37
1	1.14	1.71	1.83	1.10	2.03	2.45
2	1.17	2.77	2.85	1.06	3.23	3.29
3	1.13	3.79	3.68	1.10	4.21	4.49
4	1.15	4.92	4.90	1.14	5.40	5.41
5	1.16	5.93	5.72	1.18	6.42	6.57
6	1.17	7.01	6.96	1.24	7.40	7.49
conjecture	1	$s+1$	$s+1$	1	$s+1.5$	$s+1.5$
theory	–	$s-0.5$	s	–	$s-1$	s

Table 2: Estimated orders $-\log \varepsilon_{\text{abs}}/\log N$ of convergence with respect to the smoothness parameter s. These are derived by a least square fit of the computed errors as shown in Figure 1.

Next we are going to compare the runtime of our algorithms. Therefore, we consider the practical important case that the center points $y_1, \dots, y_{M_1}$, $M_1 = \mathcal{O}(N^{d-1})$, are located on the surface of a cylinder and that the radii $r_1, \dots, r_{M_2}$, $M_2 = \mathcal{O}(N)$, are equispaced in the interval $[0, 2]$. For this setup the numerical complexity of the quadrature based Algorithm 3 is $\mathcal{O}(N^{2d-1})$, the numerical complexity of Algorithm 1 based on the nonequispaced fast Fourier transform is $\mathcal{O}(N^{d+1} \log N)$ and the numerical complexity of Algorithm 2 based on the sparse fast Fourier transform is $\mathcal{O}(N^3 \log N)$. The numerical results are shown in Figure 2. We observe that in the two dimensional case we have nearly the same behavior for both algorithms. In the three dimensional case, however, the algorithm based on the NFFT is much faster than the quadrature based algorithm. In particlar for large N, the speedup is essential for practical applications. Unfortunately, the algorithm based on the sparse Fourier transform steps behind the NFFT based algorithm. This mostly because it was implemented in MATLAB whereas the other two methods where implemented in C. Nevertheless, the sparse Fourier transform based algorithm shows the flattest increase of the runtime as N grows up.

5 Summary

We discretised the spherical mean value operator by trigonometric polynomials, which gives rise to spectral error estimates in case of globally smooth functions. Moreover, the resulting algorithm has optimal arithmetical complexity in the important three-dimensional case and thus allows for the simulation of interesting problem sizes.

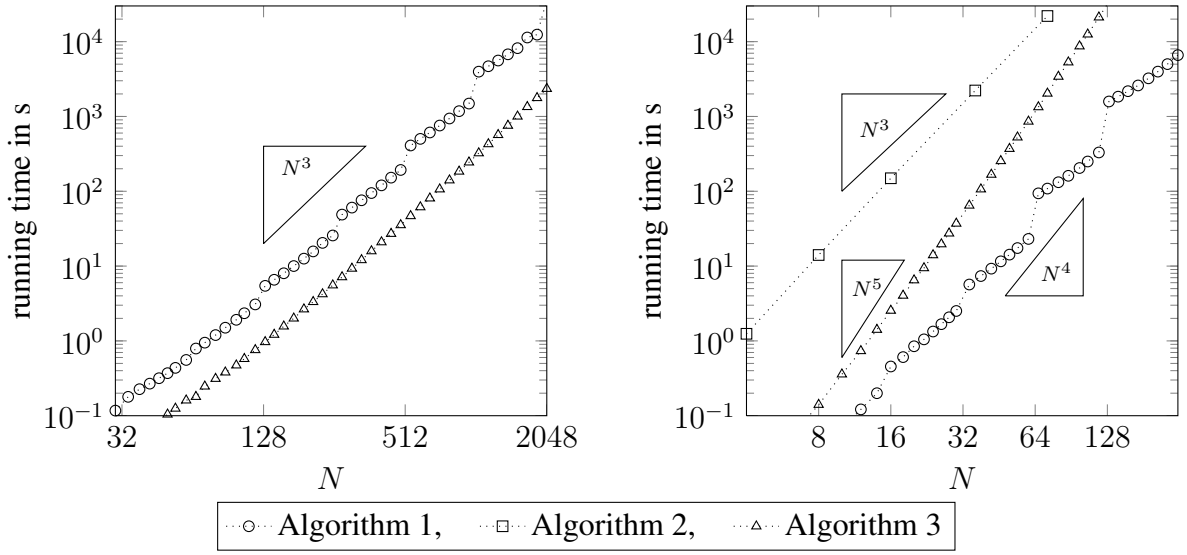

Figure 2: Running times with respect to the discretisation parameter N for spatial dimension $d = 2$ (left) and $d = 3$ (right).

Acknowledgement

The authors gratefully acknowledge support by the Helmholtz Association, contract number VH-NG-526.

References

[1] M. Agranovsky and P. Kuchment. Uniqueness of reconstruction and an inversion procedure for thermoacoustic and photoacoustic tomography with variable sound speed. *Inverse Problems*, 23(5):2089–2102, 2007.

[2] M. Agranovsky, P. Kuchment, and L. Kunyansky. On reconstruction formulas and algorithms for the thermoacoustic tomography. In L. V. Wang, editor, *Photoacoustic imaging and spectroscopy*, chapter 8, pages 89–101. CRC Press, Boca Raton, FL, 2009.

[3] M. Agranovsky, P. Kuchment, and E. T. Quinto. Range descriptions for the spherical mean Radon transform. *J. Funct. Anal.*, 248(2):344–386, 2007.

[4] A. Buehler, A. Rosenthal, T. Jetzfellner, A. Dima, D. Razansky, and V. Ntziachristos. Model-based optoacoustic inversions with incomplete projection data. *Med. Phys.*, 38(1694), 2011.

[5] P. Burgholzer, G. J. Matt, M. Haltmeier, and G. Paltauf. Exact and approximate imaging methods for photoacoustic tomography using an arbitrary detection surface. *Phys. Rev. E*, 75(4):046706, 2007.

[6] Y. Dong, T. Görner, and S. Kunis. An iterative reconstruction scheme for photoacoustic imaging. *Preprint*, 2011.

[7] F. Filbir, R. Hielscher, and W. R. Madych. Reconstruction from circular and spherical mean data. *Appl. Comput. Harmon. Anal.*, 29(1):111–120, 2010.

[8] D. Finch, M. Haltmeier, and Rakesh. Inversion of spherical means and the wave equation in even dimensions. *SIAM J. Appl. Math.*, 68(2):392–412, 2007.

[9] M. Haltmeier. A mollification approach for inverting the spherical mean radon transform. *SIAM J. Appl. Math.*, 71(5):1637–1652, 2011.

[10] M. Haltmeier, O. Scherzer, P. Burgholzer, and G. Paltauf. Thermoacoustic computed tomography with large planar receivers. *Inverse Problems*, 20(5):1663–1673, 2004.

[11] M. Haltmeier, O. Scherzer, and G. Zangerl. A reconstruction algorithm for photoacoustic imaging based on the nonuniform FFT. *IEEE Trans. Med. Imag.*, 28(11):1727–1735, 2009.

[12] M. Haltmeier, T. Schuster, and O. Scherzer. Filtered backprojection for thermoacoustic computed tomography in spherical geometry. *Math. Methods Appl. Sci.*, 28(16):1919–1937, 2005.

[13] M. Haltmeier and G. Zangerl. Spatial resolution in photoacoustic tomography: effects of detector size and detector bandwidth. *Inverse Problems*, 26(12):125002, 14, 2010.

[14] J. Keiner, S. Kunis, and D. Potts. Using NFFT 3—a software library for various nonequispaced fast Fourier transforms. *ACM Trans. Math. Software*, 36(4):Art. 19, 30, 2009.

[15] P. Kuchment and L. Kunyansky. Mathematics of thermoacoustic tomography. *European J. Appl. Math.*, 19(2):191–224, 2008.

[16] S. Kunis and I. Melzer. On the butterfly sparse Fourier transform. Preprint, 2011.

[17] L. Kunyansky. Reconstruction of a function from its spherical (circular) means with the centers lying on the surface of certain polygons and polyhedra. *Inverse Problems*, 27(2):025012, 22, 2011.

[18] L. A. Kunyansky. Explicit inversion formulae for the spherical mean Radon transform. *Inverse Problems*, 23(1):373–383, 2007.

[19] L. A. Kunyansky. A series solution and a fast algorithm for the inversion of the spherical mean Radon transform. *Inverse Problems*, 23(6):S11–S20, 2007.

[20] G. Paltauf, R. Nuster, M. Haltmeier, and P. Burgholzer. Photoacoustic tomography with integrating area and line detectors. In L. V. Wang, editor, *Photoacoustic Imaging and Spectroscopy*, Optical Science and Engineering, chapter 20, pages 251–263. CRC Press, Boca Raton, FL, 2009.

[21] E. T. Quinto. Helgason's support theorem and spherical Radon transforms. In *Radon transforms, geometry, and wavelets*, volume 464 of *Contemp. Math.*, pages 249–264. Amer. Math. Soc., Providence, RI, 2008.

[22] L. V. Wang and H. Wu. *Biomedical Optics - Principles and Imaging*. John Wiley & Sons Inc., Hoboken, NJ, 2007.

[23] G. N. Watson. *A Treatise on the Theory of Bessel Functions*. Cambridge University Press, Cambridge, GB, 1966.

[24] L. Ying. Sparse Fourier transform via butterfly algorithm. *SIAM J. Sci. Comput.*, 31(3):1678–1694, 2009.

[25] G. Zangerl and O. Scherzer. Exact reconstruction in photoacoustic tomography with circular integrating detectors II: spherical geometry. *Math. Methods Appl. Sci.*, 33(15):1771–1782, 2010.

[26] G. Zangerl, O. Scherzer, and M. Haltmeier. Exact series reconstruction in photoacoustic tomography with circular integrating detectors. *Commun. Math. Sci.*, 7(3):665–678, 2009.

Preprint Series DFG-SPP 1324

http://www.dfg-spp1324.de

Reports

[1] R. Ramlau, G. Teschke, and M. Zhariy. A Compressive Landweber Iteration for Solving Ill-Posed Inverse Problems. Preprint 1, DFG-SPP 1324, September 2008.

[2] G. Plonka. The Easy Path Wavelet Transform: A New Adaptive Wavelet Transform for Sparse Representation of Two-dimensional Data. Preprint 2, DFG-SPP 1324, September 2008.

[3] E. Novak and H. Woźniakowski. Optimal Order of Convergence and (In-) Tractability of Multivariate Approximation of Smooth Functions. Preprint 3, DFG-SPP 1324, October 2008.

[4] M. Espig, L. Grasedyck, and W. Hackbusch. Black Box Low Tensor Rank Approximation Using Fibre-Crosses. Preprint 4, DFG-SPP 1324, October 2008.

[5] T. Bonesky, S. Dahlke, P. Maass, and T. Raasch. Adaptive Wavelet Methods and Sparsity Reconstruction for Inverse Heat Conduction Problems. Preprint 5, DFG-SPP 1324, January 2009.

[6] E. Novak and H. Woźniakowski. Approximation of Infinitely Differentiable Multivariate Functions Is Intractable. Preprint 6, DFG-SPP 1324, January 2009.

[7] J. Ma and G. Plonka. A Review of Curvelets and Recent Applications. Preprint 7, DFG-SPP 1324, February 2009.

[8] L. Denis, D. A. Lorenz, and D. Trede. Greedy Solution of Ill-Posed Problems: Error Bounds and Exact Inversion. Preprint 8, DFG-SPP 1324, April 2009.

[9] U. Friedrich. A Two Parameter Generalization of Lions' Nonoverlapping Domain Decomposition Method for Linear Elliptic PDEs. Preprint 9, DFG-SPP 1324, April 2009.

[10] K. Bredies and D. A. Lorenz. Minimization of Non-smooth, Non-convex Functionals by Iterative Thresholding. Preprint 10, DFG-SPP 1324, April 2009.

[11] K. Bredies and D. A. Lorenz. Regularization with Non-convex Separable Constraints. Preprint 11, DFG-SPP 1324, April 2009.

[12] M. Döhler, S. Kunis, and D. Potts. Nonequispaced Hyperbolic Cross Fast Fourier Transform. Preprint 12, DFG-SPP 1324, April 2009.

[13] C. Bender. Dual Pricing of Multi-Exercise Options under Volume Constraints. Preprint 13, DFG-SPP 1324, April 2009.

[14] T. Müller-Gronbach and K. Ritter. Variable Subspace Sampling and Multi-level Algorithms. Preprint 14, DFG-SPP 1324, May 2009.

[15] G. Plonka, S. Tenorth, and A. Iske. Optimally Sparse Image Representation by the Easy Path Wavelet Transform. Preprint 15, DFG-SPP 1324, May 2009.

[16] S. Dahlke, E. Novak, and W. Sickel. Optimal Approximation of Elliptic Problems by Linear and Nonlinear Mappings IV: Errors in L_2 and Other Norms. Preprint 16, DFG-SPP 1324, June 2009.

[17] B. Jin, T. Khan, P. Maass, and M. Pidcock. Function Spaces and Optimal Currents in Impedance Tomography. Preprint 17, DFG-SPP 1324, June 2009.

[18] G. Plonka and J. Ma. Curvelet-Wavelet Regularized Split Bregman Iteration for Compressed Sensing. Preprint 18, DFG-SPP 1324, June 2009.

[19] G. Teschke and C. Borries. Accelerated Projected Steepest Descent Method for Nonlinear Inverse Problems with Sparsity Constraints. Preprint 19, DFG-SPP 1324, July 2009.

[20] L. Grasedyck. Hierarchical Singular Value Decomposition of Tensors. Preprint 20, DFG-SPP 1324, July 2009.

[21] D. Rudolf. Error Bounds for Computing the Expectation by Markov Chain Monte Carlo. Preprint 21, DFG-SPP 1324, July 2009.

[22] M. Hansen and W. Sickel. Best m-term Approximation and Lizorkin-Triebel Spaces. Preprint 22, DFG-SPP 1324, August 2009.

[23] F.J. Hickernell, T. Müller-Gronbach, B. Niu, and K. Ritter. Multi-level Monte Carlo Algorithms for Infinite-dimensional Integration on $\mathbb{R}^{\mathbb{N}}$. Preprint 23, DFG-SPP 1324, August 2009.

[24] S. Dereich and F. Heidenreich. A Multilevel Monte Carlo Algorithm for Lévy Driven Stochastic Differential Equations. Preprint 24, DFG-SPP 1324, August 2009.

[25] S. Dahlke, M. Fornasier, and T. Raasch. Multilevel Preconditioning for Adaptive Sparse Optimization. Preprint 25, DFG-SPP 1324, August 2009.

[26] S. Dereich. Multilevel Monte Carlo Algorithms for Lévy-driven SDEs with Gaussian Correction. Preprint 26, DFG-SPP 1324, August 2009.

[27] G. Plonka, S. Tenorth, and D. Roşca. A New Hybrid Method for Image Approximation using the Easy Path Wavelet Transform. Preprint 27, DFG-SPP 1324, October 2009.

[28] O. Koch and C. Lubich. Dynamical Low-rank Approximation of Tensors. Preprint 28, DFG-SPP 1324, November 2009.

[29] E. Faou, V. Gradinaru, and C. Lubich. Computing Semi-classical Quantum Dynamics with Hagedorn Wavepackets. Preprint 29, DFG-SPP 1324, November 2009.

[30] D. Conte and C. Lubich. An Error Analysis of the Multi-configuration Time-dependent Hartree Method of Quantum Dynamics. Preprint 30, DFG-SPP 1324, November 2009.

[31] C. E. Powell and E. Ullmann. Preconditioning Stochastic Galerkin Saddle Point Problems. Preprint 31, DFG-SPP 1324, November 2009.

[32] O. G. Ernst and E. Ullmann. Stochastic Galerkin Matrices. Preprint 32, DFG-SPP 1324, November 2009.

[33] F. Lindner and R. L. Schilling. Weak Order for the Discretization of the Stochastic Heat Equation Driven by Impulsive Noise. Preprint 33, DFG-SPP 1324, November 2009.

[34] L. Kämmerer and S. Kunis. On the Stability of the Hyperbolic Cross Discrete Fourier Transform. Preprint 34, DFG-SPP 1324, December 2009.

[35] P. Cerejeiras, M. Ferreira, U. Kähler, and G. Teschke. Inversion of the noisy Radon transform on $SO(3)$ by Gabor frames and sparse recovery principles. Preprint 35, DFG-SPP 1324, January 2010.

[36] T. Jahnke and T. Udrescu. Solving Chemical Master Equations by Adaptive Wavelet Compression. Preprint 36, DFG-SPP 1324, January 2010.

[37] P. Kittipoom, G. Kutyniok, and W.-Q Lim. Irregular Shearlet Frames: Geometry and Approximation Properties. Preprint 37, DFG-SPP 1324, February 2010.

[38] G. Kutyniok and W.-Q Lim. Compactly Supported Shearlets are Optimally Sparse. Preprint 38, DFG-SPP 1324, February 2010.

[39] M. Hansen and W. Sickel. Best m-Term Approximation and Tensor Products of Sobolev and Besov Spaces – the Case of Non-compact Embeddings. Preprint 39, DFG-SPP 1324, March 2010.

[40] B. Niu, F.J. Hickernell, T. Müller-Gronbach, and K. Ritter. Deterministic Multi-level Algorithms for Infinite-dimensional Integration on $\mathbb{R}^{\mathbb{N}}$. Preprint 40, DFG-SPP 1324, March 2010.

[41] P. Kittipoom, G. Kutyniok, and W.-Q Lim. Construction of Compactly Supported Shearlet Frames. Preprint 41, DFG-SPP 1324, March 2010.

[42] C. Bender and J. Steiner. Error Criteria for Numerical Solutions of Backward SDEs. Preprint 42, DFG-SPP 1324, April 2010.

[43] L. Grasedyck. Polynomial Approximation in Hierarchical Tucker Format by Vector-Tensorization. Preprint 43, DFG-SPP 1324, April 2010.

[44] M. Hansen und W. Sickel. Best m-Term Approximation and Sobolev-Besov Spaces of Dominating Mixed Smoothness - the Case of Compact Embeddings. Preprint 44, DFG-SPP 1324, April 2010.

[45] P. Binev, W. Dahmen, and P. Lamby. Fast High-Dimensional Approximation with Sparse Occupancy Trees. Preprint 45, DFG-SPP 1324, May 2010.

[46] J. Ballani and L. Grasedyck. A Projection Method to Solve Linear Systems in Tensor Format. Preprint 46, DFG-SPP 1324, May 2010.

[47] P. Binev, A. Cohen, W. Dahmen, R. DeVore, G. Petrova, and P. Wojtaszczyk. Convergence Rates for Greedy Algorithms in Reduced Basis Methods. Preprint 47, DFG-SPP 1324, May 2010.

[48] S. Kestler and K. Urban. Adaptive Wavelet Methods on Unbounded Domains. Preprint 48, DFG-SPP 1324, June 2010.

[49] H. Yserentant. The Mixed Regularity of Electronic Wave Functions Multiplied by Explicit Correlation Factors. Preprint 49, DFG-SPP 1324, June 2010.

[50] H. Yserentant. On the Complexity of the Electronic Schrödinger Equation. Preprint 50, DFG-SPP 1324, June 2010.

[51] M. Guillemard and A. Iske. Curvature Analysis of Frequency Modulated Manifolds in Dimensionality Reduction. Preprint 51, DFG-SPP 1324, June 2010.

[52] E. Herrholz and G. Teschke. Compressive Sensing Principles and Iterative Sparse Recovery for Inverse and Ill-Posed Problems. Preprint 52, DFG-SPP 1324, July 2010.

[53] L. Kämmerer, S. Kunis, and D. Potts. Interpolation Lattices for Hyperbolic Cross Trigonometric Polynomials. Preprint 53, DFG-SPP 1324, July 2010.

[54] G. Kutyniok and W.-Q Lim. Shearlets on Bounded Domains. Preprint 54, DFG-SPP 1324, July 2010.

[55] A. Zeiser. Wavelet Approximation in Weighted Sobolev Spaces of Mixed Order with Applications to the Electronic Schrödinger Equation. Preprint 55, DFG-SPP 1324, July 2010.

[56] G. Kutyniok, J. Lemvig, and W.-Q Lim. Compactly Supported Shearlets. Preprint 56, DFG-SPP 1324, July 2010.

[57] A. Zeiser. On the Optimality of the Inexact Inverse Iteration Coupled with Adaptive Finite Element Methods. Preprint 57, DFG-SPP 1324, July 2010.

[58] S. Jokar. Sparse Recovery and Kronecker Products. Preprint 58, DFG-SPP 1324, August 2010.

[59] T. Aboiyar, E. H. Georgoulis, and A. Iske. Adaptive ADER Methods Using Kernel-Based Polyharmonic Spline WENO Reconstruction. Preprint 59, DFG-SPP 1324, August 2010.

[60] O. G. Ernst, A. Mugler, H.-J. Starkloff, and E. Ullmann. On the Convergence of Generalized Polynomial Chaos Expansions. Preprint 60, DFG-SPP 1324, August 2010.

[61] S. Holtz, T. Rohwedder, and R. Schneider. On Manifolds of Tensors of Fixed TT-Rank. Preprint 61, DFG-SPP 1324, September 2010.

[62] J. Ballani, L. Grasedyck, and M. Kluge. Black Box Approximation of Tensors in Hierarchical Tucker Format. Preprint 62, DFG-SPP 1324, October 2010.

[63] M. Hansen. On Tensor Products of Quasi-Banach Spaces. Preprint 63, DFG-SPP 1324, October 2010.

[64] S. Dahlke, G. Steidl, and G. Teschke. Shearlet Coorbit Spaces: Compactly Supported Analyzing Shearlets, Traces and Embeddings. Preprint 64, DFG-SPP 1324, October 2010.

[65] W. Hackbusch. Tensorisation of Vectors and their Efficient Convolution. Preprint 65, DFG-SPP 1324, November 2010.

[66] P. A. Cioica, S. Dahlke, S. Kinzel, F. Lindner, T. Raasch, K. Ritter, and R. L. Schilling. Spatial Besov Regularity for Stochastic Partial Differential Equations on Lipschitz Domains. Preprint 66, DFG-SPP 1324, November 2010.

[67] E. Novak and H. Woźniakowski. On the Power of Function Values for the Approximation Problem in Various Settings. Preprint 67, DFG-SPP 1324, November 2010.

[68] A. Hinrichs, E. Novak, and H. Woźniakowski. The Curse of Dimensionality for Monotone and Convex Functions of Many Variables. Preprint 68, DFG-SPP 1324, November 2010.

[69] G. Kutyniok and W.-Q Lim. Image Separation Using Shearlets. Preprint 69, DFG-SPP 1324, November 2010.

[70] B. Jin and P. Maass. An Analysis of Electrical Impedance Tomography with Applications to Tikhonov Regularization. Preprint 70, DFG-SPP 1324, December 2010.

[71] S. Holtz, T. Rohwedder, and R. Schneider. The Alternating Linear Scheme for Tensor Optimisation in the TT Format. Preprint 71, DFG-SPP 1324, December 2010.

[72] T. Müller-Gronbach and K. Ritter. A Local Refinement Strategy for Constructive Quantization of Scalar SDEs. Preprint 72, DFG-SPP 1324, December 2010.

[73] T. Rohwedder and R. Schneider. An Analysis for the DIIS Acceleration Method used in Quantum Chemistry Calculations. Preprint 73, DFG-SPP 1324, December 2010.

[74] C. Bender and J. Steiner. Least-Squares Monte Carlo for Backward SDEs. Preprint 74, DFG-SPP 1324, December 2010.

[75] C. Bender. Primal and Dual Pricing of Multiple Exercise Options in Continuous Time. Preprint 75, DFG-SPP 1324, December 2010.

[76] H. Harbrecht, M. Peters, and R. Schneider. On the Low-rank Approximation by the Pivoted Cholesky Decomposition. Preprint 76, DFG-SPP 1324, December 2010.

[77] P. A. Cioica, S. Dahlke, N. Döhring, S. Kinzel, F. Lindner, T. Raasch, K. Ritter, and R. L. Schilling. Adaptive Wavelet Methods for Elliptic Stochastic Partial Differential Equations. Preprint 77, DFG-SPP 1324, January 2011.

[78] G. Plonka, S. Tenorth, and A. Iske. Optimal Representation of Piecewise Hölder Smooth Bivariate Functions by the Easy Path Wavelet Transform. Preprint 78, DFG-SPP 1324, January 2011.

[79] A. Mugler and H.-J. Starkloff. On Elliptic Partial Differential Equations with Random Coefficients. Preprint 79, DFG-SPP 1324, January 2011.

[80] T. Müller-Gronbach, K. Ritter, and L. Yaroslavtseva. A Derandomization of the Euler Scheme for Scalar Stochastic Differential Equations. Preprint 80, DFG-SPP 1324, January 2011.

[81] W. Dahmen, C. Huang, C. Schwab, and G. Welper. Adaptive Petrov-Galerkin methods for first order transport equations. Preprint 81, DFG-SPP 1324, January 2011.

[82] K. Grella and C. Schwab. Sparse Tensor Spherical Harmonics Approximation in Radiative Transfer. Preprint 82, DFG-SPP 1324, January 2011.

[83] D.A. Lorenz, S. Schiffler, and D. Trede. Beyond Convergence Rates: Exact Inversion With Tikhonov Regularization With Sparsity Constraints. Preprint 83, DFG-SPP 1324, January 2011.

[84] S. Dereich, M. Scheutzow, and R. Schottstedt. Constructive quantization: Approximation by empirical measures. Preprint 84, DFG-SPP 1324, January 2011.

[85] S. Dahlke and W. Sickel. On Besov Regularity of Solutions to Nonlinear Elliptic Partial Differential Equations. Preprint 85, DFG-SPP 1324, January 2011.

[86] S. Dahlke, U. Friedrich, P. Maass, T. Raasch, and R.A. Ressel. An adaptive wavelet method for parameter identification problems in parabolic partial differential equations. Preprint 86, DFG-SPP 1324, January 2011.

[87] A. Cohen, W. Dahmen, and G. Welper. Adaptivity and Variational Stabilization for Convection-Diffusion Equations. Preprint 87, DFG-SPP 1324, January 2011.

[88] T. Jahnke. On Reduced Models for the Chemical Master Equation. Preprint 88, DFG-SPP 1324, January 2011.

[89] P. Binev, W. Dahmen, R. DeVore, P. Lamby, D. Savu, and R. Sharpley. Compressed Sensing and Electron Microscopy. Preprint 89, DFG-SPP 1324, March 2011.

[90] P. Binev, F. Blanco-Silva, D. Blom, W. Dahmen, P. Lamby, R. Sharpley, and T. Vogt. High Quality Image Formation by Nonlocal Means Applied to High-Angle Annular Dark Field Scanning Transmission Electron Microscopy (HAADF-STEM). Preprint 90, DFG-SPP 1324, March 2011.

[91] R. A. Ressel. A Parameter Identification Problem for a Nonlinear Parabolic Differential Equation. Preprint 91, DFG-SPP 1324, May 2011.

[92] G. Kutyniok. Data Separation by Sparse Representations. Preprint 92, DFG-SPP 1324, May 2011.

[93] M. A. Davenport, M. F. Duarte, Y. C. Eldar, and G. Kutyniok. Introduction to Compressed Sensing. Preprint 93, DFG-SPP 1324, May 2011.

[94] H.-C. Kreusler and H. Yserentant. The Mixed Regularity of Electronic Wave Functions in Fractional Order and Weighted Sobolev Spaces. Preprint 94, DFG-SPP 1324, June 2011.

[95] E. Ullmann, H. C. Elman, and O. G. Ernst. Efficient Iterative Solvers for Stochastic Galerkin Discretizations of Log-Transformed Random Diffusion Problems. Preprint 95, DFG-SPP 1324, June 2011.

[96] S. Kunis and I. Melzer. On the Butterfly Sparse Fourier Transform. Preprint 96, DFG-SPP 1324, June 2011.

[97] T. Rohwedder. The Continuous Coupled Cluster Formulation for the Electronic Schrödinger Equation. Preprint 97, DFG-SPP 1324, June 2011.

[98] T. Rohwedder and R. Schneider. Error Estimates for the Coupled Cluster Method. Preprint 98, DFG-SPP 1324, June 2011.

[99] P. A. Cioica and S. Dahlke. Spatial Besov Regularity for Semilinear Stochastic Partial Differential Equations on Bounded Lipschitz Domains. Preprint 99, DFG-SPP 1324, July 2011.

[100] L. Grasedyck and W. Hackbusch. An Introduction to Hierarchical (H-) Rank and TT-Rank of Tensors with Examples. Preprint 100, DFG-SPP 1324, August 2011.

[101] N. Chegini, S. Dahlke, U. Friedrich, and R. Stevenson. Piecewise Tensor Product Wavelet Bases by Extensions and Approximation Rates. Preprint 101, DFG-SPP 1324, September 2011.

[102] S. Dahlke, P. Oswald, and T. Raasch. A Note on Quarkonial Systems and Multilevel Partition of Unity Methods. Preprint 102, DFG-SPP 1324, September 2011.

[103] A. Uschmajew. Local Convergence of the Alternating Least Squares Algorithm For Canonical Tensor Approximation. Preprint 103, DFG-SPP 1324, September 2011.

[104] S. Kvaal. Multiconfigurational time-dependent Hartree method for describing particle loss due to absorbing boundary conditions. Preprint 104, DFG-SPP 1324, September 2011.

[105] M. Guillemard and A. Iske. On Groupoid C*-Algebras, Persistent Homology and Time-Frequency Analysis. Preprint 105, DFG-SPP 1324, September 2011.

[106] A. Hinrichs, E. Novak, and H. Woźniakowski. Discontinuous information in the worst case and randomized settings. Preprint 106, DFG-SPP 1324, September 2011.

[107] M. Espig, W. Hackbusch, A. Litvinenko, H. Matthies, and E. Zander. Efficient Analysis of High Dimensional Data in Tensor Formats. Preprint 107, DFG-SPP 1324, September 2011.

[108] M. Espig, W. Hackbusch, S. Handschuh, and R. Schneider. Optimization Problems in Contracted Tensor Networks. Preprint 108, DFG-SPP 1324, October 2011.

[109] S. Dereich, T. Müller-Gronbach, and K. Ritter. On the Complexity of Computing Quadrature Formulas for SDEs. Preprint 109, DFG-SPP 1324, October 2011.

[110] D. Belomestny. Solving optimal stopping problems by empirical dual optimization and penalization. Preprint 110, DFG-SPP 1324, November 2011.

[111] D. Belomestny and J. Schoenmakers. Multilevel dual approach for pricing American style derivatives. Preprint 111, DFG-SPP 1324, November 2011.

[112] T. Rohwedder and A. Uschmajew. Local convergence of alternating schemes for optimization of convex problems in the TT format. Preprint 112, DFG-SPP 1324, December 2011.

[113] T. Görner, R. Hielscher, and S. Kunis. Efficient and accurate computation of spherical mean values at scattered center points. Preprint 113, DFG-SPP 1324, December 2011.